Title
Invariant natural killer T cells coordinate removal of senescent cells

Permalink
https://escholarship.org/uc/item/8s321168

Authors
Arora, Shivani
Thompson, Peter J
Wang, Yao
et al.

Peer reviewed

Invariant Natural Killer T cells coordinate removal of senescent cells

Shivani Arora[#,1], **Peter J. Thompson**[#,1,5], **Yao Wang**[1], **Aritra Bhattacharyya**[2,4], **Hara Apostolopoulou**[1], **Rachel Hatano**[3], **Ram P. Naikawadi**[2], **Ajit Shah**[3], **Paul J Wolters**[2], **Suneil Koliwad**[1], **Mallar Bhattacharya**[2,4], **Anil Bhushan**[1]

[1]Diabetes Center, University of California San Francisco, San Francisco CA, USA 94143

[2]Division of Pulmonary and Critical Care, Department of Medicine, University of California San Francisco, San Francisco CA, USA 94143

[3]Deciduous Therapeutics, MBC Biolabs, San Francisco, CA, USA 94107

[4]The Sandler Asthma Basic Research Center, University of California San Francisco, San Francisco, CA, USA 94143

[#] These authors contributed equally to this work.

Summary

Background—The failure of immune surveillance to remove senescent cells drive age-related diseases. Here, we target an endogenous immune surveillance mechanism that can promote elimination of senescent cells and reverse disease progression.

Methods—We identify a class of lipid-activated T cells, invariant natural killer T cells (iNKTs) are involved in the removal of pathologic senescent cells. We use two disease models in which senescent cells accumulate to test whether activation of iNKT cells was sufficient to eliminate senescent cells in vivo.

Findings—Senescent preadipocytes accumulate in white adipose tissue of chronic high-fat diet (HFD) fed mice, and activation of iNKT cells with the prototypical glycolipid antigen alpha-galactosylceramide (αGalCer) led to a reduction of these cells with improved glucose control. Similarly, senescent cells accumulate within the lungs of mice injured by inhalational

---

bleomycin, and αGalCer-induced activation of iNKT cells greatly limited this accumulation, decreased the lung fibrosis and improved survival. Furthermore, co-culture experiments showed that the preferential cytotoxic activity of iNKT cells to senescent cells is conserved in human cells.

Conclusions—These results uncover a senolytic capacity of tissue-resident iNKT cells and pave the way for anti-senescence therapies that target these cells and their mechanism of activation.

eTOC Blurb:

Senescent cells accumulate within tissues and drive the progression of diseases. Arora et al. identify an endogenous immune surveillance mechanism to uncover a senolytic capacity of tissue-resident iNKT cells and pave the way for anti-senescence therapies that target these cells and their mechanism of activation.

Graphical Abstract:
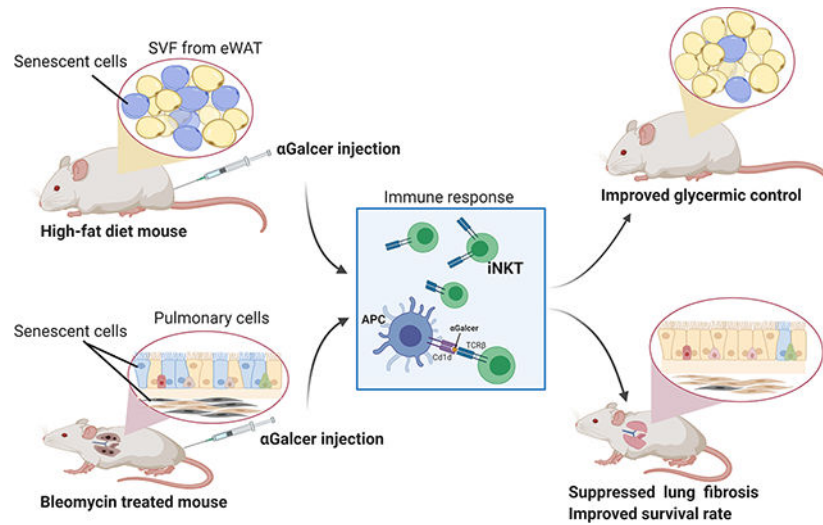
Keywords

Senescence; iNKT cells; Fibrosis; IPF; Metabolic dysfunction; senolytic

Introduction

The accumulation of senescent cells within tissues can drive the progression of diseases[1,2]. While removal of senescent cells with senolytic drugs has emerged as a promising therapeutic approach, the ubiquitous target of these drugs makes clinical applications challenging. In healthy tissue, endogenous immune surveillance mechanisms limit the build-up of senescent cells by targeted removal of senescent cells[3]. The failure of the immune surveillance to efficiently recognize and target senescent cell clearance could result in the accumulation of senescent cells. The identity of the endogenous immune surveillance that mediated senescent cell clearance in vivo is not clear.

To address this question, we looked for tissues that showed accumulation of senescent cells in vivo. Senescent preadipocytes were reported to accumulate in the white adipose

tissue (WAT) of both mice chronically fed a HFD[4] and in obese humans[8]. Genetic ablation (of p16[Ink4a]-expressing cells) or use of senolytic compounds resulted in the elimination of senescent preadipocytes[4,15,16], suggesting that we could use HFD mice as a model to investigate immune surveillance in senescent preadipocyte clearance. To identify mechanisms mediating immune surveillance of such senescent cells in the WAT, we looked for upregulated cell surface receptors that could mediate interactions between senescent cells and immune cells[6,7]. Using single-cell analysis, we previously showed that mRNA encoding beta-2-microglobulin (B2M), a component of the class I major histocompatibility complex (MHC), is highly upregulated in senescent beta cells[9], leading us here to explore class I MHC-like molecules among preadipocytes from the WAT of mice. We identified an MHC Class I-like molecule CD1d, that is normally expressed by antigen-presenting cells but showed elevated expression specifically in the senescent preadipocytes suggesting a potential link between senescence and immune regulation.

CD1d in complex with B2M presents lipid antigens to a class of T lymphocytes known as invariant Natural Killer T (iNKT) cells[10]. iNKT cells have an invariant T cell receptor (TCR) and are readily identified in both humans and mice with antigen-loaded CD1d tetramers, making this a population of T cells that has been comprehensively surveyed[11,12]. iNKT cells decline in frequency and function in humans with age[13,14], but a link between this decrease and the increase in senescent cells during aging or disease has not been hypothesized or investigated. Here we describe how lipid antigen-presentation to activate iNKT cells can constitute an endogenous surveillance system that can be manipulated to clear senescent cells in disease models.

Results

Senescent cells accumulate in eWAT of HFD mice

To characterize obesity-associated senescent cells in the epididymal WAT (eWAT), we fed male mice a HFD (60% kcal from fat) for 16 weeks (from 6 weeks until 22 weeks of age) and then isolated the stromal vascular fraction (SVF) associated with the eWAT, which is comprised predominantly of preadipocytes (~75%), but also includes mesenchymal stem cells and endothelial cells[17] along with resident immune cells. We depleted the immune cells from SVF using CD45 antibody-labeled nanobeads prior to probing for senescent cells in both chow-fed (control) and HFD-fed mice. We then measured senescence-associated-βgal (SA-βgal) activity[18] and the mRNA levels of genes associated with senescence and the senescence-associated secretory phenotype (SASP)[19] in the remaining SVF cells (Fig. 1a). This preadipocyte-enriched population, when isolated from obese mice, consistently showed increased SA-βgal staining and elevated expression of several senescence *(Cdkn2a[Ink4a], Il6)* genes, whereas those from age-matched control mice did not (Fig. 1b and 1c). This was similar to when comparing proliferative and senescent preadipocytes (Suppl Fig. 1a–b). Consistent with the upregulation of CD1d on senescent preadipocytes in vitro (Suppl Fig. 1c), we found CD1d expression was increased in preadipocytes isolated from HFD fed mice compared to chow mice (Fig. 1d).

$C_{12}FDG^{Hi}$ cells mark secretory senescent cells that are sensitive to senolytics

To quantify the number of senescent preadipocytes from the eWAT of obese vs. lean mice, we used a common flow cytometric assay that measures SA-βgal activity with the fluorogenic substrate $C_{12}FDG^{20}$ (Fig. 1e). Based on median fluorescence intensity of $C_{12}FDG$, we identified a subpopulation of CD45$^-$ CD31$^-$ preadipocytes from the SVF of HFD mice that had elevated SA-βgal activity when compared to those from control diet-fed counterparts (Fig. 1f). The CD31$^+$ cells did not appear to contribute significantly to the overall $C_{12}FDG$ signal, and subsequently, we used the CD45$^-$ negative gating to characterize the senescent cells (Fig. 1g–h). We next explored whether SA-βgal activity levels could distinguish different subsets of senescent cells, we used, we used FACS to separate preadipocytes from HFD fed mice and separated the high fluorescence (highest ~25%, $C_{12}FDG^{Hi}$) from those with low fluorescence (lowest ~20%, $C_{12}FDG^{Lo}$) (Fig. 2a) such that the levels of $C_{12}FDG$ fluorescence were ~30-fold higher in the $C_{12}FDG^{Hi}$ vs. $C_{12}FDG^{Lo}$ population (Fig. 2b). While *Cdkn1a* and *Cdkn2a^{Ink4a}* were expressed at the same levels in both these preadipocyte subsets, $C_{12}FDG^{Hi}$ cells had elevated mRNA levels of secretory genes that comprise SASP such as *Il6* and *Ccl2* relative to $C_{12}FDG^{Lo}$ cells from the same obese mice (Fig. 2c). We designated the $C_{12}FDG^{Lo}$ cells as replicative senescent and $C_{12}FDG^{Hi}$ as secretory senescent cells.

We next tested whether these $C_{12}FDG^{Hi}$ preadipocytes could be ablated with senolytic drugs. The Bcl2 family is known to be upregulated in senescent cells, and ABT-737, a BH3 mimetic that is well-tolerated *in vivo,* acts as a senolytic by inducing apoptosis preferentially in senescent cells[21]. We found that senescent preadipocytes upregulated Bcl-xL (Suppl Fig. 2) suggesting that they would be sensitive to ABT-737. HFD-fed and control mice were treated with ABT-737, and we quantified $C_{12}FDG^{Hi}$ preadipocytes from the SVF of their eWAT. Treatment with ABT-737 reduced the number of $C_{12}FDG^{Hi}$ cells and concordantly increased the relative number of $C_{12}FDG^{Lo}$ cells, within the preadipocyte-enriched population of the SVF from the eWAT of HFD-fed mice when compared to vehicle-treated controls (Fig. 2d and 2e).

α-GalCer treatment results in activation and expansion of iNKT in eWAT

We next considered whether iNKT cells could similarly regulate the numbers of secretory senescent cells within the WAT of obese mice. We first quantified the number of tissue-resident iNKT cells in the eWAT of both chow- and HFD-fed mice using a CD1d tetramer loaded with α-GalCer to specifically detect these cells (Fig. 3a). Using this approach, we found that the number of iNKT cells normalized to total live SVF cells within the eWAT was consistently reduced in the context of diet-induced obesity (Fig. 3b). Treatment of HFD mice with alpha-Galactosylceramide (α-GalCer), a well-known lipid antigen that specifically activates iNKT cells when presented on CD1d *in vitro* and *in vivo*[10] was sufficient to dramatically increase iNKT cell numbers compared with similarly obese mice treated with vehicle (Fig. 3b and 3c). In contrast with ABT-737, α -GalCer itself did not affect the viability of senescent preadipocytes in vitro (Suppl Fig. 3a–b), suggesting that it does not eliminate senescent cells via a direct cytotoxic effect. This finding is consistent with the activation of iNKT cells in the eWAT by α-GalCer treatment.

α-GalCer treatment of HFD mice leads to removal of senescent cells and normalizes blood glucose

To explore whether activation of iNKT regulates senescent cells, we treated mice with α-GalCer and assess the senescent cells in the SVF fraction of eWAT. We injected HFD mice with either α-GalCer or vehicle and analyzed SA-βgal activity among eWAT-derived SVF cells by FACS for $C_{12}FDG$ (Fig. 3a). As expected, mice with diet-induced obesity injected with the vehicle, had an increased frequency of $C_{12}FDG^{Hi}$ preadipocytes in the eWAT relative to that seen in lean mice fed the control diet. By contrast, treating obese mice with α-GalCer was remarkably in its ability to deplete the number of these $C_{12}FDG^{Hi}$ cells to levels akin to those seen in lean control mice (Fig. 3d). We also tested whether the α-GalCer-induced activation of iNKT cells was required for the removal of senescent cells. We used *Traj18*-deficient mice that lack the invariant chain of the T cell receptor[39]. HFD fed WT and *Traj18*^{−/−} mice were injected with α-GalCer and C12FDG+ SVF cells were used to assess senescent cells. α-GalCer treatment resulted in reduction of senescent cells in WT HFD mice but failed to reduce senescent cells in *Traj18*^{−/−} mice (Suppl Fig 4). To assess the effect of eliminating senescent cells on metabolic health, we monitored blood glucose and insulin levels in HFD-fed mice treated with α-GalCer. HFD-fed mice that received α-GalCer had significantly lower fasting glucose, improved glucose tolerance, and improved insulin sensitivity compared to vehicle-treated HFD-fed mice and resembled chow-fed mice (Fig. 3e and 3f).

Adoptive transfer of activated iNKT leads to reduced senescent preadipocytes in HFD mice

To confirm that the clearance of WAT senescent cells in response to in vivo α-GalCer delivery was mediated by activated iNKT cells as opposed to any off-target effects, we assessed the ability of adoptively transferred eWAT-isolated iNKT cells to clear senescent cells from the eWAT of recipient mice rendered obese by prior HFD feeding. iNKT cells were FACS-isolated from the eWAT of α-GalCer-treated HFD mice using the CD1d-loaded tetramer, and ~150–300,000 of these iNKT cells were transferred into recipient mice in two separate experiments (Fig. 3h). Remarkably, such transfer was sufficient to markedly deplete the number of $C_{12}FDG^{Hi}$ preadipocytes otherwise present in the eWAT of HFD-fed control recipient mice relative to untreated controls. Notably, the effect of adoptive transfer phenocopied that of treating HFD-fed mice with α-GalCer directly, which was used as a positive control for these experiments (Fig. 3i–j). Together these data directly implicate the involvement of activated resident eWAT iNKT cells in the clearance of senescent preadipocytes in a model where they accumulate in the WAT.

Activation of iNKT in an IPF model results in decreased senescent cells and reduced fibrosis.

To address the generality of iNKT-mediated clearance of senescent cells and whether such mechanisms operate in other disease settings, we turned to the lung and investigated bleomycin-induced injury, a model for interstitial lung disease[22]. Intratracheal instillation of the chemotherapeutic agent bleomycin induces epithelial damage, followed by infiltration of inflammatory cells into the lung interstitium and alveolar space[23]. Previous studies have demonstrated that senescent epithelial and mesenchymal cells accumulate after bleomycin-

induced injury and that senolytic treatment can clear these senescent cells[5]. Accumulation of senescent epithelial cells also occurs in lung tissue of patients with idiopathic lung fibrosis (IPF), and senolytic treatment in an open-label study of IPF patients showed benefit suggesting that the bleomycin-induced injury is a good model for senolytic approaches to lung fibrosis[24].

To test whether iNKT cells could eliminate senescent cells in bleomycin-induced lung injury model, we carried out bleomycin-induced injury in a cohort of C57BL6 male mice. Ten days after injury, these mice were either treated systemically with α-GalCer or left untreated, while age-matched uninjured mice treated with the vehicle on day 10 served as controls (Fig. 4a). Lungs were harvested 14 days after injury, and the proportion of senescent epithelial and mesenchymal cells was quantified, as was the relative number of iNKT cells. As seen in WAT-associated preadipocytes from HFD-fed mice, bleomycin-induced lung injury induced a marked increase in the number of senescent $CD45^-$ lung cells, as analyzed by quantifying SA-βgal activity using the $C_{12}FDG$ assay (Fig. 4b). Importantly, α-GalCer treatment of bleomycin-injured mice decreased the number of such $CD45^- C_{12}FDG^+$ lung cells to levels on par with those in the lungs of uninjured control mice (Fig. 4b). As with previous studies using a cocktail of senolytics[5], both epithelial and mesenchymal senescent cells were affected by α-GalCer treatment (Suppl Fig. 5). To confirm that the changes in SA-βgal activity reflected senescent cells, we analyzed mRNA levels of senescence and SASP markers. Consistent with the $C_{12}FDG$ assay, $CD45^-$ lung cells from bleomycin-injured mice had increased mRNA levels of senescence *(Cdkn2a^Ink4a)* and SASP *(Ccl2, Serpine1)* markers. Moreover, α-GalCer treatment of bleomycin-injured mice reduced mRNA levels of these marker genes, consistent with the diminished SA-βgal activity we observed using the $C_{12}FDG$ assay (Fig. 4c). As in the eWAT, α-GalCer treatment also induced expansion of lung parenchymal iNKT cells in the context of bleomycin-induced injury (Fig. 4d). To address whether this iNKT expansion and its associated senolytic effect also suppressed lung fibrosis, we used the hydroxyproline (HP) assay[22] to measure whole lung collagen content in bleomycin-injured mice treated with or without α-GalCer. Importantly, α-GalCer treatment of lung-injured mice significantly reduced lung hydroxyproline content, consistent with suppressed fibrosis (Fig. 4e). Removal of senescence and suppression of fibrosis has beneficial effects on survival as mortality of α-GalCer-injected mice was significantly reduced compared to the vehicle-injected mice (Fig. 4f). These findings are generally consistent with earlier work[25,26], although these studies were more preventative rather than therapeutic as either α-GalCer or adoptively transferred iNKT cells was administered prior to bleomycin injury, potentially mitigating the development of lung injury rather than reversing fibrosis after it was established[27]. Importantly, these prior studies did not evaluate or link their observed effects to a reduction of senescent cells. Taken together, these results suggest that iNKT cell activation within the lung by α-GalCer treatment attenuates the accumulation of senescent cells during bleomycin-induced IPF, producing an anti-fibrotic effect and improved survival.

Activated iNKT cells are preferentially cytotoxic to human senescent cells

To address whether iNKT cells can directly act on senescent cells in humans, we developed an *in vitro* cytotoxicity assay. Peripheral blood mononuclear cells (PBMCs) from a healthy

human donor were used to both generate dendritic cells (DCs) and isolate iNKT cells, which were then cultured separately. In parallel, human lung fibroblasts (WI-38) were cultured and treated with etoposide to induce senescence. Untreated proliferating WI-38 cells were used as controls. α-GalCer-loaded DCs were used to activate and expand iNKT cells. We combined activated iNKTs with either senescent or proliferative (untreated) WI-38 cells in co-cultures and employed the xCELLigence platform[28] to measure cellular impedance, and thus, continuously monitor real-time kinetic behavior indicative of cell number and attachment. The non-specific kinase inhibitor staurosporine, which induces rapid apoptosis independently of cell state, was used as a positive control for cytotoxicity (data not shown). Senescent or proliferating WI-38 cells were seeded into wells, and activated iNKT cells were added to these wells at different target-to-effector ratios. iNKT cells remain in suspension and do not adhere to the wells and as such contribute negligibly to impedance. Using the xCELLigence software, the percent cytolysis was calculated and used for comparing the relative efficacy of activated iNKT towards senescent and non-senescent WI-38 target cells (Fig. 4g). Co-culture of activated iNKT cells with proliferative WI-38 cells showed minimal cell killing at two target:effector ratios. By contrast, co-culturing similarly activated iNKT cells with senescent WI-38 cells induced a significant dose and time-dependent increase in cytolysis of senescent fibroblasts, reaching a maximum of ~100% at both target:effector ratios by 18 h (Fig. 4h). Moreover, even at the lowest target:effector ratio of 1:2, activated iNKT were significantly more cytotoxic towards senescent cells at both the midpoint (8 h) and endpoints (18 h) of the assay (Fig. 4i). These results indicate that activated primary human iNKT cells can preferentially induce cytotoxicity of senescent over proliferative cells.

Discussion

Senescence phenotypes vary depending on the context and trigger, and it is apparent that different immune cell types co-operate to remove senescent cells in different tissues. For instance, NK cells mediate surveillance of senescent activated stellate cells in the liver[29], and recent work has shown that the perforin-granzyme pathway is vital for cytotoxic effector function in the elimination of senescent cells in multiple tissues during aging and chemically induced liver fibrosis[30,31]. A recent paper leveraged the expression of a urokinase-type plasminogen activator receptor (uPAR) on oncogene-induced senescent cells to develop antigen-specific CAR-T cells that could ablate the senescent population[32] This approach to senolysis may be well suited to situations where senescent cells express an aberrant antigen in a particular tissue context, such as in oncogene-induced senescence associated with cancer, but not in chronic diseases associated with DNA damage-induced senescence as we could not identify uPAR on senescent preadipocytes in the HFD mice (data not shown). We overcome the reliance on antigen specificity by using iNKT cells here as the means to achieve effective senolysis, and by doing so could clear senescent cells of different types in different tissue environments despite a common delivery method. iNKT cells have both adaptive and innate features that make them uniquely suited to coordinating an early response to the elimination of aberrant cells, such as virus-infected cells or senescent cells. Activation of iNKT cells with α-GalCer has been found to reverse adverse metabolic phenotypes in the HFD mouse model[33–35] as well as the fibrosis induced by lung injury[26,27].

Our results provide the first evidence that iNKT cells can eliminate senescent cells in these two distinct models where tissue dysfunction is dependent on the accumulation of senescent cells[4,15,16,5,26,27].

While senolytics have been the dominant approach to move senescence-clearing therapies to the clinic, several reasons make the activation of iNKT cells a promising approach. Senolytics target anti-apoptotic pathways that are upregulated not only in senescent cells, but these pathways can also be active in non-senescent cells. To avoid toxicity, clinical trials with senolytics are administered locally to reduce the risk of side effects. In contrast, the unique invariant TCR on iNKT cells allows exquisite specificity for lipid antigens such as α-GalCer, and our results demonstrate that iNKT cell activation by α-GalCer renders them specifically cytotoxic to senescent rather than non-senescent cells. Another advantage is that the activation of iNKTs is short-lived, avoiding an unchecked and prolonged cytolytic effect[10]. Pre-clinical and clinical studies evaluating the safety of α-GalCer showed that it has generally been well-tolerated over a wide range of doses with minimal side effects[11]. Taken together along with the results presented here, these considerations suggest that specific activation of surveillance responses by iNKT cells provides a rationale for developing the next generation of approaches to eliminate inflammatory senescent cells associated with chronic diseases.

Limitations of Study

The upregulation of CD1d on senescent cells led us to the identification of iNKT cells, however, it is not clear whether CD1d is sufficient for iNKT cells to recognize senescent cells. Since CD1d is primarily expressed on antigen-expressing cells, the exact mechanism by which iNKT cells target senescent cells and the role of CD1d in activation or inhibition of iNKT cells requires further investigation[40]. It is also important to note that activation of iNKT cells produce cytokines that can modulate the local immune response and as such, in addition to direct cytotoxicity, iNKTs may also have indirect effects in vivo. Thus, while this study does not indicate a direct role for other cell types such as NK cells or T effector cells in immune surveillance of senescent cells in these models, this possibility cannot be conclusively ruled out.

STAR Method Text

RESOURCE AVAILABILITY

Lead Contact.—Further information and requests for resources and reagents should be directed to and will be fulfilled by the lead contact, Anil Bhushan (Bhushan.lab@ucsf.edu)

Materials Availability.—This study did not generate any new or unique materials.

Data and Code Availability.—This study did not generate/analyze datasets or code.

EXPERIMENTAL MODEL AND SUBJECT DETAILS

Mouse husbandry.—All procedures involving mice were performed according to the IACUC standards following ethics approval by the animal committee at the University of

California San Francisco. Male C57BL6/J on chow or HFD fed mice were purchased from Jackson Labs (cat. no 380050). HFD mice were fed a high-fat diet (60% kcal from fat) from 6 weeks until 22 weeks of age. All experiments on HFD mice were performed at 22–24 weeks total age (16–18 weeks on HFD). Age-matched male C57BL6/J mice on standard rodent chow diet were used as controls. Transgenic luciferase mice (CAG-Luc) were purchased from Jackson Labs. Mice were housed in a specific pathogen-free facility with a 12-hour light-dark cycle at 23°C. For the lung injury model, 10-week-old male C57BL/6J mice (Jackson Labs) were used. The animals were divided into three groups: the control group, the injured group, and the α-GalCer treated group. The animals in the control group received vehicle only (i.p.) on day 10. The injured group animals received bleomycin (3U/kg) via the intratracheal route at the start of the experiment (day 0). The animals in the α-GalCer treated groups received bleomycin (3U/kg) on day 0, and i.p. injection of α-GalCer (2 μg/mouse) on day 10. The animals in all the groups were sacrificed on day 14, and lungs were harvested for isolation of primary pulmonary Alveolar Type II cells (ATII) on the same day. For the hydroxyproline assay, mice were euthanized 21 days after injury.

Epidydmal white adipose tissue stromal vascular fraction (eWAT SVF) isolation.—eWAT SVF was isolated using standard protocols. Briefly, mice were euthanized, and epididymal fat pads were harvested, washed twice in D-PBS and minced. eWAT pads were digested with 1 U/ml Collagenase-D (Roche) in 1XHBSS containing 1 % BSA (Sigma-Aldrich) for 1 hr at 37°C. Digested fat tissue was then strained twice through 100 μm strainers and neutralized with 30 ml of complete culture media (DMEM-F12 1:1, 10% FBS, IXPenicillin-streptomycin). Samples were spun at 500g for 5 minutes, shaken to resuspend the SVF pellet and then spun again. The resulting SVF pellet containing blood cells was lysed with ACKS buffer, washed in D-PBS and spun down. Total live SVF cells were counted using trypan blue and then used for various assays.

Isolation of primary epithelial cells from lung.—Primary epithelial cells from murine lungs were isolated as per the method described by Sinah and Lowell[36] with slight modifications. Briefly, mice were euthanized with an overdose of isoflurane. A bilateral thoracotomy was performed, and lungs were exsanguinated by perfusion with PBS containing 5mM EDTA via right ventricle after snipping left atrium. Following perfusion, lungs were instilled with 50 units/mL Dispase II (Thermo Fisher Scientific, Cat #17105041) via tracheal cannulation and allowed to sit for 5 min. Lungs were excised from the thoracic cavity and digested in dispase at 37°C for 45min. Cells were released from the lungs by gentle teasing and collected in sterile DMEM (Gibco; Cat # 12320032) containing DNase I (1mg/10mL, Sigma; Cat # D5025-150KU). To get the single-cell suspension, lung homogenate was sequentially filtered through 70μm and 40μm cell strainers and centrifuged at 300g for 10mins at 4°C. RBCs in cell pellet were lysed by resuspending in 1 mL ACK lysis buffer (Gibco, A10492–01) for 3 min and was neutralized using 10 mL of sterile DMEM medium, centrifuged and the cell pellet resuspended in 1 ml of sterile DMEM containing DNase I. Viability of the cells was analyzed using Vi-Cell XR cell viability analyzer.

CD45+ cell depletion of eWAT SVF.—eWAT SVF, as prepared above, was depleted of CD45+ cells using metal-assisted cell sorting (MACS) nanobeads (BioLegend) according to the product protocol. The CD45-depleted (unmagnetized) fraction was collected, spun down at 500g for 5 minutes and either plated on tissue-culture treated plates for X-gal staining or used for RNA extraction with Trizol. For lung cells, ATII cells ($<10^7/100$ μl) were washed with MojoSort buffer and were incubated with 10 μl of mouse CD45 Nanobeads for 15 mins on ice. After incubation, cells were washed with MojoSort buffer, centrifuged at 300g for 5 min, then resuspended in 3ml of MojoSort buffer in polypropylene tubes, and placed in the magnetic column for 15 mins at 4°C. After 15 mins, the 2.5 ml of supernatant was collected as the unlabeled or CD45-depleted fraction. The cells in the CD45-depleted fraction were centrifuged at 300g for 5 min and were stored in 300 μl of TRI reagent (Zymo Research) at −80°C until RNA extraction.

X-Gal staining for SA-βgal activity.—Inguinal WAT preadipocytes or eWAT SVF from chow or HFD mice, depleted of CD45+ cells and plated for 24 h were stained for SA-βgal activity using X-gal with a commercial kit (Cell Signaling Technology) according to the product instructions. Images were taken at 10X or 20X on a bright-field microscope.

C_{12}FDG flow cytometry assay.—eWAT SVF cells isolated and counted as described above were adjusted to 3×10^6 cells/ml in complete culture media and incubated with 33 μM C_{12}FDG (MarkerGene) for 1 hr in a 37°C water bath. Cells were then spun down at 500g for 5 minutes, washed with Cell Staining buffer (BioLegend), and stained with anti-CD45-APC (clone 30F-11) and anti-CD31-PE-Cy7 (clone 390) (BioLegend) each at a 1:200 dilution on ice for 30 minutes. Cells were then washed in Cell Staining buffer and resuspended in Cell Staining buffer containing 1X 7-AAD (Cayman Chemical). Samples were analyzed on an Attune acoustic focusing cytometer. Gates were set as follows: cells (FSC-A/SSC-A), forward scatter singlets (FSC-H/FSC-A), side-scatter singlets (SSC-H/SSC-A), live cells (7-AAD⁻), non-immune cells (CD45⁻), non-endothelial cells (CD31⁻) and analyzed for C_{12}FDG fluorescence. In some cases, CD31 was not included, as we had found that the inclusion or exclusion of this population did not significantly change the overall distribution or gating of the C_{12}FDG subpopulations. Data were analyzed with FlowJo (v.10). For Lung, 1×10^6 cells from each sample were used to perform the assay. The cells were incubated with 66μm of C_{12}FDG (Markergene) in sterile DMEM containing DNase for 1 hour at 37°C. Following the incubation, the cells were washed with Cell Staining buffer (Biolegend, 420201), blocked with anti CD16/32 mouse monoclonal antibody (1:1000, prepared by the UCSF monoclonal antibody core), and stained with APC anti-mouse CD45 (1:400, Biolegend, 103112), and 7-AAD (1:1000, Cayman Chemical, 400201). The gating strategy followed selected 7-AAD⁻, CD45⁻, and C12FDG+ cells.

Flow cytometry for CD1d.—Ing or eWAT preadipocytes from CAG-Luc mice at different passages were collected and stained with anti-CD1-PE (clone 1B1) in Cell Staining buffer (BioLegend). Flow cytometry was then performed on the Attune acoustic focusing cytometer. Gates were set as follows: cells (FSC-A/SSC-A), forward scatter singlets (FSC-H/FSC-A), live cells (GFP+), and CD1d fluorescence.

α-GalCer activation of iNKT cells.—iNKT cells were activated in vivo using α-GalCer as described previously[14]. Briefly, HFD mice were i.p. injected with 200 μl of a 10 μg/ml α-GalCer solution (2 μg total) made up in 5.6% Sucrose, 5%Tween-20. On day 3 or 4 post-injection, mice were euthanized for various experiments, as indicated.

Flow cytometry of iNKT cells.—eWAT SVF cells were stained with PBS57 (α-GalCer-analog) loaded onto CD1d-PE tetramers prepared by the NIH Tetramer Core and anti-CD3-APC (clone 17A2, BioLegend). As a negative control for subtracting background staining in eWAT SVF, samples were also stained with unloaded CD1d-PE tetramer and anti-CD3-APC. Live cells were enumerated with DAPI, and flow cytometry was performed on an Attune acoustic focusing cytometer. Gates were set to identify: cells (FSC-A/SSC-A), forward scatter singlets (FSC-H/FSC-A), side-scatter singlets (SSC-H/SSC-A), live cells (DAPI⁻), and the PBS57::CD1d-PE⁺/CD3-APC⁺ subpopulation. The percent of unloaded CD1d-PE⁺/CD3-APC⁺ cells were subtracted from the loaded tetramer stained populations to eliminate the percent of background stained cells. For lung, 1×10^6 cells from each sample were used to quantify iNKT cells. The incubation, the cells were washed with cell staining buffer (Biolegend, 420201), blocked with anti CD16/32 mouse monoclonal antibody (1:1000), and were stained with DAPI (1:2000, Thermo Scientific,), Tetramer (α-GalCer loaded CD1d tetramer, NIH) labeled with PE (1:100); APC labeled anti mouse CD3 (1:400, BioLegend, 100236). The gating strategy followed is DAPI negative, CD3 and Tetramer double positive. The iNKT-Cell count is reported as the percentage of CD3 cells staining positive with the tetramer.

Metabolic measurements.—Seventeen male HFD-fed C57BL6J mice were divided into the vehicle (n=8) and the α-GalCer treated group (n=9). Age-matched male C57BL6/J mice on a standard rodent chow diet were used as controls (n=8). A glucose tolerance test was performed 10 days after α-GalCer injection. Mice were fasted overnight (14h) before being injecting 2g/kg glucose intraperitoneally. Blood glucose was measured at 0, 15, 30, 60, and 120 min after glucose injection using a glucometer (Abbott Diabetes Care Inc., Alameda, CA).

Bleomycin lung injury.—For measurement of lung collagen, 3 U/kg Bleomycin (Meitheal) was instilled intratracheally, with injection of α-GalCer or vehicle at day 10, followed by lung harvest for hydroxyproline assay at 20 days. For the survival study, 4 U/kg Bleomycin (Meitheal) was instilled intratracheally, with injection of α-GalCer or vehicle at day 5.

Adoptive transfer of iNKT cells.—HFD mice were treated with α-GalCer as described above and then on day 3 sacrificed followed by eWAT SVF isolation, iNKT cell staining, and flow cytometry were carried out as described above. Approximately 150–300,000 Live iNKT cells were sorted on a Sony SH800S flow sorter, into lymphocyte media (RPMI-1640, 10% FBS, 1X antibiotic-antimycotic). Sort purity was generally 90%. Cells were then immediately spun down (500g for 5 minutes) reconstituted in 150–200 μl D-PBS and i.p. injected into recipient HFD mice. Alongside the adoptive transfer, HFD mice were left untreated as negative controls or were treated with α-GalCer as above, to serve as positive

controls. On day 4 post-transfer, HFD mice were euthanized, and C_{12}FDG assays were carried out on the eWAT SVF.

Flow sorting of C_{12}FDG^{Hi} and C_{12}FDG^{Lo} cells from eWAT SVF.—WAT SVF was isolated from HFD mice and stained using the C_{12}FDG staining procedure with anti-CD45-APC (clone 30F-11) to gate out immune cells and DAPI to identify live cells. Samples were sorted on a Sony SH800S sorter. Gates were set to identify: cells (FSC-A/SSC-A), forward scatter singlets (FSC-W/FSC-A), side-scatter singlets (SSC-W/SSC-A), live cells (DAPI$^-$), non-immune cells (CD45$^-$) for C12FDG fluorescence. The C12FDG histogram plot was then gated on the top ~25% highest fluorescent subpopulation (C_{12}FDG^{Hi}) and the lowest ~20% (C_{12}FDG^{Lo}) and sorted into two different tubes containing Trizol for RNA extraction.

Hydroxyproline Assay.—Hydroxyproline assay was performed as have been described earlier[37]. Briefly, snap-frozen lung samples were homogenized and mixed with 50% Trichloroacetic acid (Sigma) before incubating them overnight in 12 M HCl at 110°C. The following day, the samples were reconstituted with water for 2 h. After reconstitution, they were mixed with 1.4% Chloramine T (Sigma) in 10% isopropanol (Fisher Scientific) and 0.5 M Sodium acetate (Sigma). Finally, they were mixed with Ehrlich's solution (Sigma) and incubated at 65°C for 15 mins. Absorbance was measured at 550 nm and the values were computed from the standard curve.

RNA extraction and Quantitative reverse transcriptase PCR.—RNA was extracted with Trizol reagent using the Zymogen total RNA micro-prep kit (Zymogen) according to the product instructions. Total RNA was quantified by Nanodrop. Approximately 200–300 ng of total RNA was used for cDNA synthesis using the qScript cDNA synthesis kit (QuantaBio). cDNA (250 ng) was diluted 1:5 before amplification with Power-UP SYBR reagent using the ABI 384-well QuantStudio 5 Real-time PCR system or Bio-Rad quantitative PCR platform (96-well format). Quantification was performed using with the delta-delta C_T method, using Cyclophilin A (*Ppia*) as a housekeeping gene.

In vitro cytotoxicity assay with human peripheral blood iNKT cells.—Human peripheral blood mononuclear cell (PBMC) iNKT isolation and expansion were based on a previous method[38]. PBMCs were isolated from healthy patients using the SepMate™ PBMC isolation system (STEMCELL Technologies). The isolation of CD14$^+$ and CD14$^-$ cells was performed using the EasySep human CD14 positive selection kit (STEMCELL Technologies). CD14$^+$ and CD14$^-$ cells were cultured with recombinant proteins: 20 ng/mL GM-CSF and 20 ng/mL IL-4, or 10U/mL IL-2 respectively (BioLegend). Basal media consisted of RPMI-1640 containing 1% sodium pyruvate, 1% non-essential amino acid solution, 1% L-glutamine, 1% antibiotic antimycotic, 1% HEPES, and 10% fetal bovine serum (complete media). On day five, the CD14$^+$ cells were treated with 0.05 mg/mL of mitomycin C at 5×10^6 cells/mL for 30 min. at 37°C, before being washed 3 times with Dulbecco's PBS (Gibco). Cells were then loaded with 200 ng/mL α-GalCer for one hour. iNKT cells were isolated from the CD14$^-$ cell population using the anti-iNKT microbeads (Miltenyi). The α-GalCer-loaded dendritic cells and iNKTs were co-cultured at a ratio of 5:1. Half media changes were performed every other day with complete media supplemented

with 20 U/mL IL-2. On day 12, cells were stained with anti-Vα24 and anti-Vβ11 (Beckman Coulter) and sorted for double-positive cells on a FACS Aria II cell sorter. The isolated iNKTs recovered for 24 hours in complete media containing 20 U/ml of IL-2. WI-38 human lung fibroblasts (ATCC) were cultured to 70% confluence in media containing Eagle's Minimum Essential Medium with 1% antibiotic antimycotic and 10% FBS (maintenance media). 100μM of etoposide was added to the media for 48 hours to induce senescence. Maintenance media was changed every other day for 6 days. 5 μg/ml of fibronectin was coated on each well of an E-Plate 96 PET (Agilent) for 20 min. On the seventh day post-senescence induction, proliferating control and etoposide-treated senescent WI-38 cells were seeded onto the plate at 5000 cells/well using Accutane. Cells were incubated with 100 μl/well of maintenance media for 1 hour at 25°C before going into the xCELLigence cradle. Twenty-four hours later, iNKT cells in complete media + 20 U/ml of IL-2 were added at ratios of 2:1 (10,000 cells) or 5:1 (25,000 cells). As a full lysis control, 1 μM of staurosporine was added to both WI-38 and etoposide-treated senescent WI-38 cells. Electrical impedance was measured every 30 min over 24 hours and normalized to the starting value (normalized cell index). For the data analysis, the time-points from 30 min (where the signal is stable) to 6 hours was used. The %cytolysis was calculated using (Eq.1), on the xCELLigence RTCA Software Pro (ACEA Biosciences Inc.). Normalized WI-38 and etoposide-treated senescent WI-38 conditions were compared to their corresponding conditions with effector iNKT cells at each time point.

$$\% \, Cytolysis \; = \; \frac{(Cell \, Index_{\text{no effector}} - Cell \, Index_{\text{effector}})}{Cell \, Index_{no \, effector}} x 100 \qquad \text{Eq.1}$$

QUANTIFICATION AND STATISTICAL ANALYSIS

For each experiment, the number of biological replicates (n) is indicated in the figure legend. Statistical comparisons were performed between groups of mice, and/or samples with n 3 biological replicates or mice, using two-tailed T-tests for two groups, or one-way ANOVA, or two-way ANOVA for three or more groups, with corrections for multiple testing. $P < 0.05$ was considered significant.

Supplementary Material

Refer to Web version on PubMed Central for supplementary material.

Acknowledgements.

References

1. Pignolo RJ, Passos JF, Khosla S, Tchkonia T & Kirkland JL Reducing Senescent Cell Burden in Aging and Disease. Trends Mol. Med 26, 630–638 (2020). [PubMed: 32589933]

2. Childs BG Gluscevic M, Baker DJ, Laberge RM, Marquess D, Dananberg J, & van Deursen JM (2017). Senescent cells: An emerging target for diseases of ageing. Nat. Rev. Drug Discov 16, 718–735. [PubMed: 28729727]

3. Kale A, Sharma A, Stolzing A, Desprez PY, & Campisi J (2020). Role of immune cells in the removal of deleterious senescent cells. Immun. Ageing 17, 1–9. [PubMed: 31911808]

4. Palmer AK, Xu M, Zhu Y, Pirtskhalava T, Weivoda MM, Hachfeld CM, Prata LG, van Dijk TH, Verkade E, Casaclang-Verzosa G, et al. (2019). Targeting senescent cells alleviates obesity-induced metabolic dysfunction. Aging Cell 18, 1–15.

5. Schafer MJ, White TA, Iijima K, Haak AJ, Ligresti G, Atkinson EJ, Oberg AL, Birch J, Salmonowicz H, Zhu Y, et al. (2017). Cellular senescence mediates fibrotic pulmonary disease. Nat. Commun 8, 14532. [PubMed: 28230051]

6. Pereira B.l. Devine OP, Vukmanovic-Stejic M, Chambers ES, Subramanian P, Patel N, Virasami A, Sebire NJ, Kinsler V, Valdovinos, et al. (2019). Senescent cells evade immune clearance via HLA-E-mediated NK and CD8+ T cell inhibition. Nat. Commun 10, 2387. 10.1038/s41467-019-10335-5. [PubMed: 31160572]

7. Sagiv A Burton DG, Moshayev Z, Vadai E, Wensveen F, Ben-Dor S, Golani O, Polic B, & Krizhanovsky V (2016). NKG2D ligands mediate immunosurveillance of senescent cells. Aging (Albany. NY). 8, 328–344. [PubMed: 26878797]

8. Gustafson B, Nerstedt A & Smith U, (2019). Reduced subcutaneous adipogenesis in human hypertrophic obesity is linked to senescent precursor cells. Nat. Commun 10, 1–9. [PubMed: 30602773]

9. Thompson PJ, Shah A, Ntranos V, Van Gool F, Atkinson M, & Bhushan A (2019). Targeted Elimination of Senescent Beta Cells Prevents Type 1 Diabetes. Cell Metab 29, 1045–60. [PubMed: 30799288]

10. Crosby CM & Kronenberg M,(2018). Tissue-specific functions of invariant natural killer T cells. Nat. Rev. Immunol 18, 559–574. [PubMed: 29967365]

11. Wolf BJ, Choi JE & Exley MA, (2018). Novel Approaches to Exploiting Invariant NKT Cells in Cancer Immunotherapy. Frontiers in Immunology 9, 384. [PubMed: 29559971]

12. Venkataswamy MM & Porcelli SA, (2010). Lipid and glycolipid antigens of CD1d-restricted natural killer T cells. Semin. Immunol 22, 68–78. [PubMed: 19945296]

13. Jing Y Gravenstein S, Chaganty NR, Chen N, Lyerly KH, Joyce S, & Deng Y, (2007). Aging is associated with a rapid decline in frequency, alterations in subset composition, and enhanced Th2 response in CD1d-restricted NKT cells from human peripheral blood. Exp. Gerontol 42, 719–732. [PubMed: 17368996]

14. Peralbo E. DelaRosa O, Gayoso I, Pita ML, Tarazona R, & Solana R, (2006). Decreased frequency and proliferative response of invariant V α24Vβ11 natural killer T (iNKT) cells in healthy elderly. Biogerontology 7, 483–492. [PubMed: 16953330]

15. Xu M, Palmer AK, Ding H, Weivoda MM, Pirtskhalava T, White TA, Sepe A, Johnson KO, Stout MB, Giorgadze N, Jensen MD, et al. , (2015). Targeting senescent cells enhances adipogenesis and metabolic function in old age. Elife 4, 1–19.

16. Xu M Xu M, Pirtskhalava T, Farr JN, Weigand BM, Palmer AK, Weivoda MM, Inman CL, Ogrodnik MB, Hachfeld CM, Fraser DG, et al. , (2018). Senolytics improve physical function and increase lifespan in old age. Nat. Med 24, 1246–56. [PubMed: 29988130]

17. Church C, Berry R & Rodeheffer MS (2014). Isolation and study of adipocyte precursors. Methods Enzymol 537, 31–46. [PubMed: 24480340]

18. Dimri GP, Lee X, Basile G, Acosta M, Scott G, Roskelley C, Medrano EE, Linskens M, Rubelj I, & Pereira-Smith O (1995). A biomarker that identifies senescent human cells in culture and in aging skin in vivo. Proc. Natl. Acad. Sci 92 (20), 9363–9367. [PubMed: 7568133]

19. He S & Sharpless NE (2017). Senescence in Health and Disease. Cell 169, 1000–1011. [PubMed: 28575665]

20. Debacq-Chainiaux F, Erusalimsky JD, Campisi J & Toussaint O (2009). Protocols to detect senescence-associated beta-galactosidase (SA-betagal) activity, a biomarker of senescent cells in culture and in vivo. Nat. Protoc 4, 1798–806. [PubMed: 20010931]

21. Yosef R, Pilpel N, Tokarsky-Amiel R, Biran A, Ovadya Y, Cohen S, Vadai E, Dassa L, Shahar E, Condiotti R, et al. (2016). Nat. Commun 7, 11190. [PubMed: 27048913]

22. Jenkins RG, Moore BB, Chambers RC, Eickelberg O, Königshoff M, Kolb M, Laurent GJ, Nanthakumar CB, Olman MA, Pardo, et al. , (2017). An official American thoracic society workshop report: Use of animal models for the pre-clinical assessment of potential therapies for pulmonary fibrosis. Am. J. Respir. Cell Mol. Biol 56, 667–679. [PubMed: 28459387]

23. Bivas-Benita M, Zwier R, Junginger HE & Borchard G, (2005). Non-invasive pulmonary aerosol delivery in mice by the endotracheal route. Eur. J. Pharm. Biopharm 61, 214–218. [PubMed: 16039104]

24. Justice JN, Nambiar AM, Tchkonia T, LeBrasseur NK, Pascual R, Hashmi SK, Prata L, Masternak MM, Kritchevsky SB, Musi N, & Kirkland JL (2019). Senolytics in idiopathic pulmonary fibrosis: Results from a first-in-human, open-label, pilot study. EBioMedicine 40, 554–563. [PubMed: 30616998]

25. Kimura T, Ishii Y, Morishima Y, Shibuya A, Shibuya K, Taniguchi M, Mochizuki M, Hegab AE, Sakamoto T, Nomura A, & Sekizawa K (2004) Treatment with α-Galactosylceramide Attenuates the Development of Bleomycin-Induced Pulmonary Fibrosis. J. Immunol 172, 5782–5789. [PubMed: 15100325]

26. Kim JH, Kim HY, Kim S, Chung JH, Park WS, & Chung DH (2005). Natural killer T (NKT) cells attenuate bleomycin-induced pulmonary fibrosis by producing interferon-gamma. The American journal of pathology, 167(5), 1231–1241. [PubMed: 16251408]

27. Blackwell TS, Tager AM, Borok Z, Moore BB, Schwartz DA, Anstrom KJ, Bar-Joseph Z, Bitterman P, Blackburn MR, Bradford,. et al. (2014). Future directions in idiopathic pulmonary fibrosis research. An NHLBI workshop report. Am. J. Respir. Crit. Care Med 189, 214–222. [PubMed: 24160862]

28. Cerignoli F, Abassi YA, Lamarche BJ, Guenther G, Santa Ana D, Guimet D, Zhang W, Zhang J, & Xi B (2018). In vitro immunotherapy potency assays using real-time cell analysis. PLoS One 13, 1–21.

29. Krizhanovsky V, Yon M, Dickins RA, Hearn S, Simon J, Miething C, Yee H, Zender L, & Lowe SW (2008). Senescence of activated stellate cells limits liver fibrosis. Cell, 134(4), 657–667. [PubMed: 18724938]

30. Ovadya Y, Landsberger T, Leins H, Vadai E, Gal H, Biran A, Yosef R, Sagiv A, Agrawal A, Shapira A,et al. (2018). Impaired immune surveillance accelerates accumulation of senescent cells and aging. Nat. Commun 9, 5435. [PubMed: 30575733]

31. Sagiv A, Biran A, Yon M, Simon J, Lowe SW, & Krizhanovsky V (2013). Granule exocytosis mediates immune surveillance of senescent cells. Oncogene 32, 1971–1977. [PubMed: 22751116]

32. Amor C, Feucht J, Leibold J, Ho YJ, Zhu C, Alonso-Curbelo D, Mansilla-Soto J, Boyer JA, Li X, Giavridis T, Kulick, et al. (2020). Senolytic CAR T cells reverse senescence-associated pathologies. Nature. doi: 10.1038/s41586-020-2403-9

33. Lynch L, Nowak M, Varghese B, Clark J, Hogan AE, Toxavidis V, Balk SP, O'Shea D, O'Farrelly C, & Exley MA (2012). Adipose Tissue Invariant NKT Cells Protect against Diet-Induced Obesity and Metabolic Disorder through Regulatory Cytokine Production. Immunity 37, 574–587. [PubMed: 22981538]

34. Schipper HS, Rakhshandehroo M, van de Graaf SF, Venken K, Koppen A, Stienstra R, Prop S, Meerding J, Hamers N, Besra G, et al. (2012). Natural killer T cells in adipose tissue prevent insulin resistance. J. Clin. Invest 122, 3343–3354. [PubMed: 22863618]

35. Ji Y, Sun S, Xu A, Bhargava P, Yang L, Lam KS, Gao B, Lee CH, Kersten S, & Qi L (2012). Activation of natural killer T cells promotes M2 macrophage polarization in adipose tissue and improves systemic glucose tolerance via interleukin-4 (IL-4)/STAT6 protein signaling axis in obesity. J. Biol. Chem. 287, 13561–13571. [PubMed: 22396530]

36. Sinha M & Lowell CA (2016). Isolation of Highly Pure Primary Mouse Alveolar Epithelial Type II Cells by Flow Cytometric Cell Sorting. Bio-protocol 6, (2016). Bio-protocol, 6(22), e2013. 10.21769/BioProtoc.2013 [PubMed: 28180137]

37. Henderson NC, Arnold TD, Katamura Y, Giacomini MM, Rodriguez JD, McCarty JH, Pellicoro A, Raschperger E, Betsholtz C, Ruminski PG, et al. (2013). Targeting of αv integrin identifies a core molecular pathway that regulates fibrosis in several organs. Nat. Med 19, 1617–1624. [PubMed: 24216753]

38. Li X, Tsuji M, Schneck J & Webb TJ (2013). Generation of Human iNKT Cell Lines. Bio-protocol 3 (6): e418. DOI: 10.21769/BioProtoc.418 [PubMed: 27570795]

39. Chandra S, Zhao M, Budelsky A, de Mingo Pulido A, Day J, Fu Z, Siegel L, Smith D, Kronenberg M (2015). A new mouse strain for the analysis of invariant NKT cell function. Nat Immunol 16(8):799–800. [PubMed: 26075912]

40. Tan AH, Chong WP, Ng SW, Basri N, Xu S, & Lam KP (2014). Aberrant presentation of self-lipids by autoimmune B cells depletes peripheral iNKT cells. Cell reports, 9(1), 24–31. [PubMed: 25263549]

Context and Significance

Failure of endogenous immune surveillance mechanisms to remove senescent cells drives the progression of diseases. The identity of the endogenous immune surveillance that mediated senescent cell clearance in vivo is not clear. This paper describes how lipid antigen-presentation to activate iNKT cells can constitute an endogenous surveillance system that can be manipulated to clear senescent cells in disease models. In two different senescence-associated disease models, activation of iNKT cells was sufficient to eliminate senescent cells in vivo and confer disease improvement. These results uncover a senolytic capacity of tissue-resident iNKT cells and pave the way for anti-senescence therapies that target these cells and their mechanism of activation.

Highlights

- Activation of invariant natural killer T cells eliminated senescent cells in vivo.

- Removal of senescent preadipocytes improves glucose control in obese mice.

- Removal of senescent cells decreased lung fibrosis and improved survival.

- Human iNKT cells were preferentially cytotoxic to senescent lung fibroblasts.
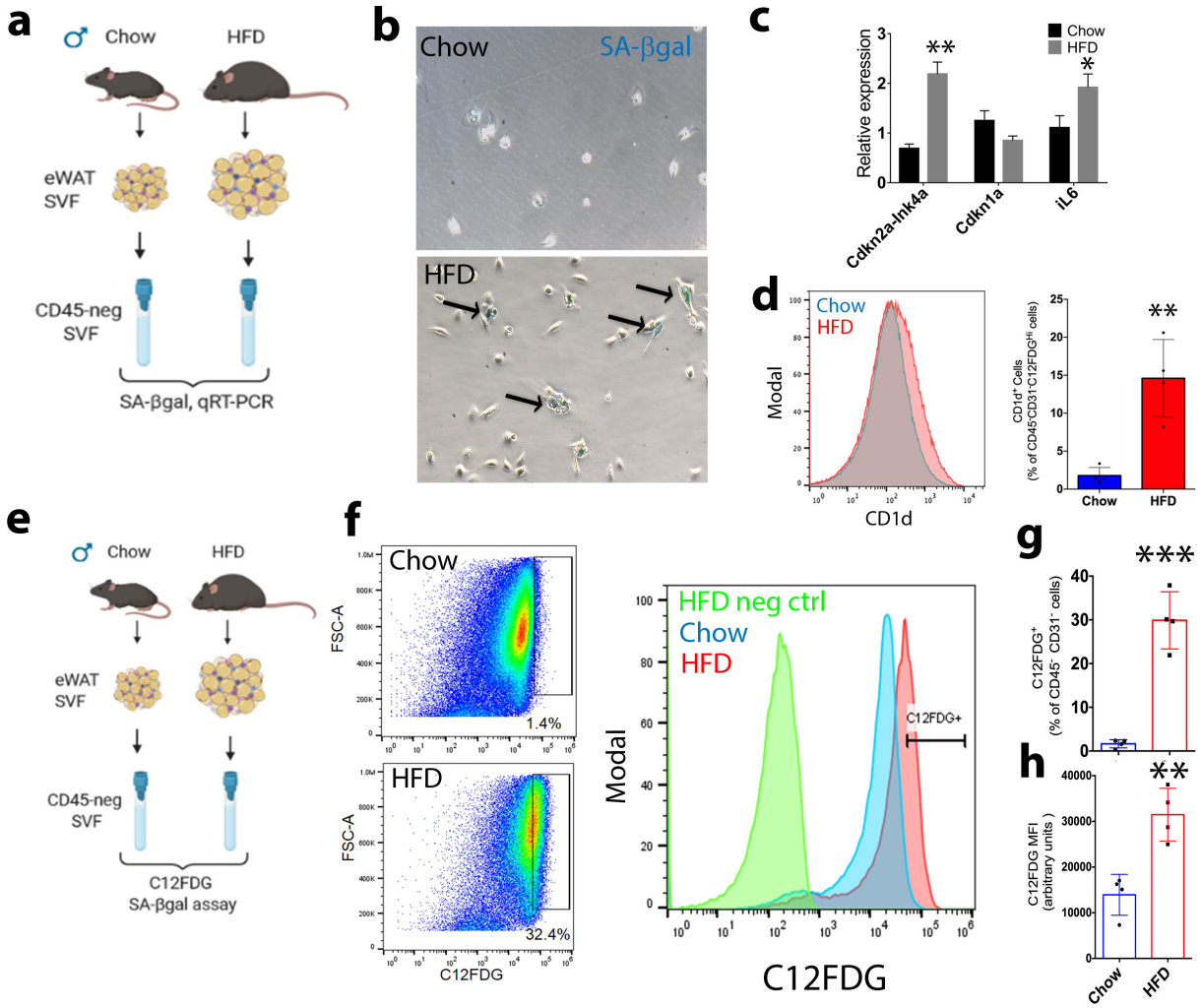
Figure 1. Senescent preadipocytes are defined by high SA-βgal activity and accumulate in white adipose tissue of HFD mice.

(a) eWAT SVF cells was isolated from chow or HFD mice (16 weeks on HFD) and depleted of CD45$^+$ cells leaving a CD45$^-$ SVF population (CD45$^-$) for X-gal staining to detect SA-βgal and qRT-PCR.

(b) X-gal staining for SA-βgal activity on CD45-depleted eWAT SVF cells isolated from chow and HFD mice.

(c) qRT-PCR of senescence markers on CD45-depleted eWAT SVF cells from chow and HFD mice. Data are mean ± SEM from n = 6 mice for each group.

(d) CD1d expression on the eWAT SVF isolated from chow and HFD mice. The cells were stained with antibodies for CD45 and CD31 (to gate out immune and endothelial cells) along with the fluorogenic substrate C$_{12}$FDG and anti-CD1d antibody. The senescent preadipocytes (DAPI-CD45$^-$CD31$^-$ C12FDG^{Hi}) were then gated for relative CD1d expression. Quantification of CD1d expression from the CD45$^-$ CD31$^-$ C12FDG^{Hi} subset from chow and HFD mice is shown in the right panel. Data are represented as mean ± SD from n=4 per experiment.

(e) eWAT SVF was isolated from chow and HFD mice and stained with antibodies for CD45 and CD31 (to gate out immune and endothelial cells) along with the fluorogenic substrate $C_{12}FDG$ to detect SA-βgal activity.

(f) Representative dot-plot showing the cell size (FSC-A) and percent of cells with the highest $C_{12}FDG$ expression in chow and HFD mice in the $CD45^-$, $CD31^-$ subpopulation. The representative histogram shows $C_{12}FDG$ staining and gating on the subset with the highest fluorescence ($C_{12}FDG^+$) in the same $CD45^-$, $CD31^-$ subpopulation.

(g) Quantification of $C_{12}FDG^+$ cells from chow or HFD mice. Data are mean ± SD from n = 4 mice per group.

(h) Quantification of the $C_{12}FDG$ MFI of the entire $CD45^-CD31^-$ population in the same chow and HFD mice as in (g). Data are mean ± SD from n = 4 mice per group.
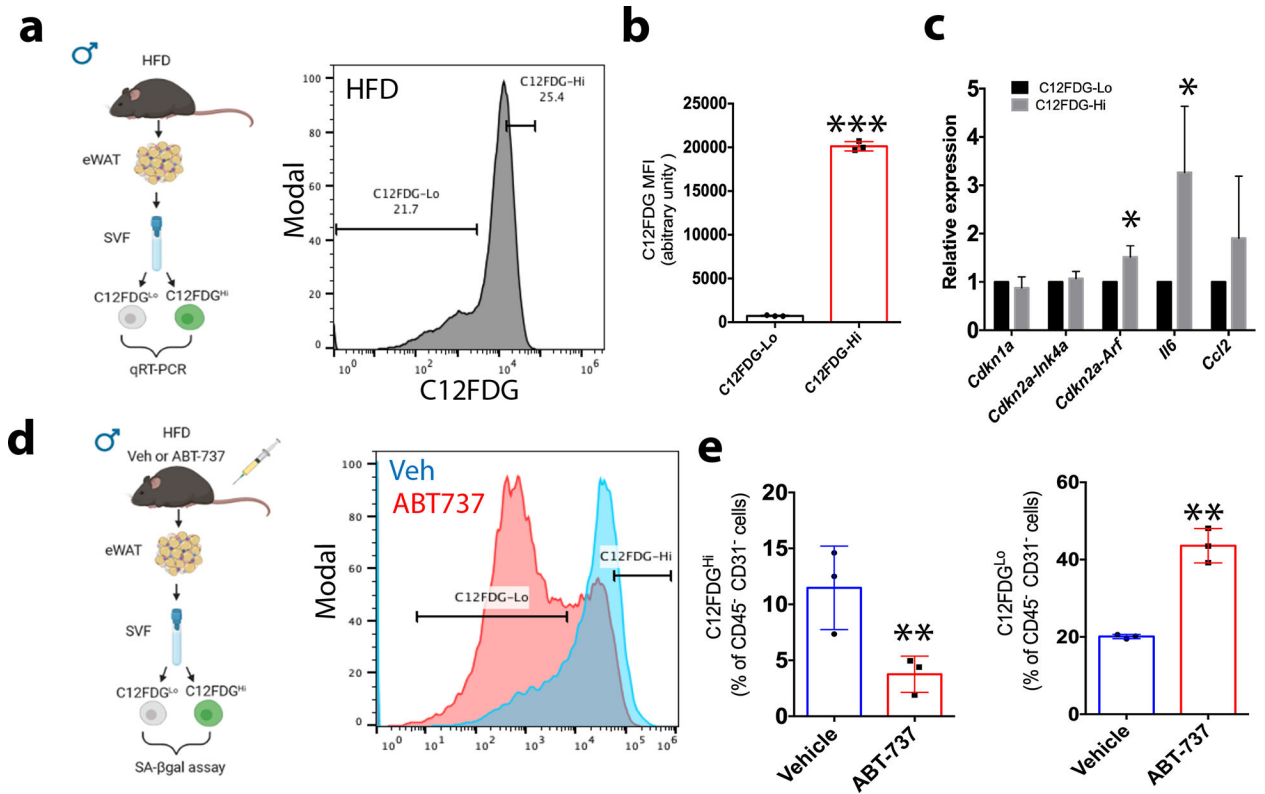
*p < 0.05, **p < 0.005, ***p< 0.0005, two-tailed T-tests.

Figure 2. Senescent preadipocytes with high SA-βgal activity express SASP genes and are preferentially eliminated with senolytic treatment.

(a) FACS was performed to isolate the $CD45^-$, $C_{12}FDG^{Lo}$ and $C_{12}FDG^{Hi}$ subpopulations from eWAT SVF of HFD mice for qRT-PCR. Shown is a representative histogram of $CD45^-$ population showing the $C_{12}FDG$ subpopulations sorted.

(b) $C_{12}FDG$ MFI of the $C_{12}FDG^{Lo}$ and $C_{12}FDG^{Hi}$ populations as shown from (g). Data are mean $\pm$ SD from n = 3 mice per group.

(c) qRT-PCR of senescence markers in $C_{12}FDG^{Hi}$ relative to $C_{12}FDG^{Lo}$ cells from the same HFD mice. Data are mean $\pm$ SD from n = 3 mice per group.

(d) HFD mice were treated with ABT-737 or vehicle for 1 week prior to harvest of eWAT SVF for the $C_{12}FDG$ assay. Shown is a representative histogram of $CD45^-$, $CD31^-$ population $C_{12}FDG$ staining.

(e) Quantification of the positive cells in the $C_{12}FDG^{Hi}$ and $C_{12}FDG^{Lo}$ subsets from vehicle and ABT-737 treated HFD mice. Data are mean $\pm$ SD from n = 3 mice per group.

*p < 0.05, **p < 0.005, ***p <0.0005, two-tailed T-tests.

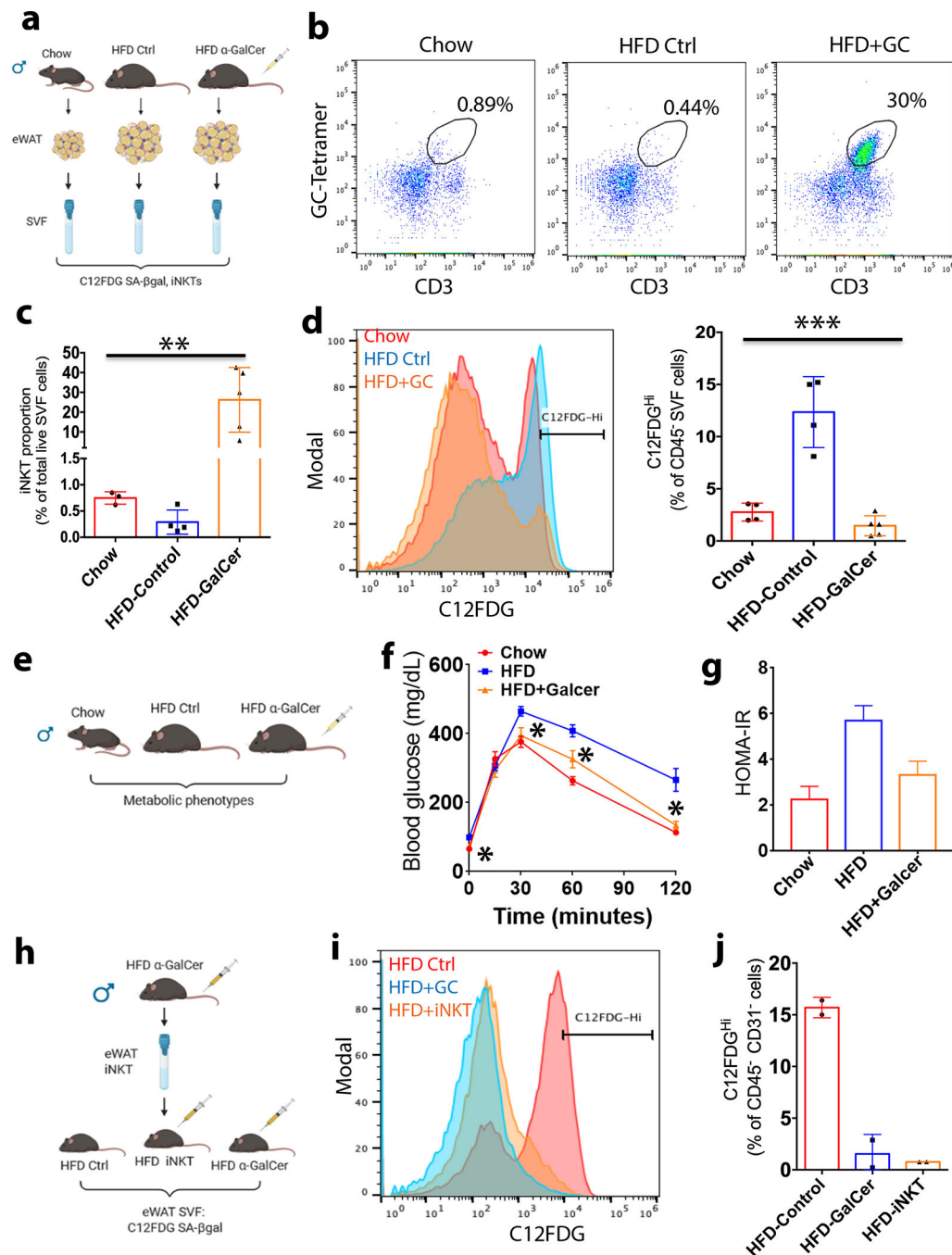**Figure 3. Activation of iNKT cells leads to clearance of senescent cells in white adipose tissue of HFD mice.**

(a) eWAT was Isolated and the SVF prepared from age-matched Chow, HFD untreated controls (HFD Ctrl), or HFD treated with α-GalCer on day 4 (HFD+GC) and senescent cells were enumerated with the C₁₂FDG SA-βgal assay while iNKT cells were enumerated with GC loaded CD1d Tetramer and anti-CD3.

(b) Representative dot plots of iNKT cell percentages from total live eWAT SVF cells, defined as GC loaded CD1d-Tetramer (GC-Tetramer)$^+$/CD3$^+$ cells In representative Chow, HFD Ctrl and HFD+GC mice.

(c) Quantification of the iNKT cell percentages in Chow (n=3), HFD Ctrl (n=4) and HFD+GC (n=5) mice per group. Data are mean ± SD.

(d) Representative histograms of $C_{12}FDG$ fluorescence and quantification of the $C_{12}FDG^{Hi}$ subpopulation of CD45$^-$ cells from Chow (n = 4), HFD Ctrl (n=5) and HFD+GC (n=5) mice per group. Data are mean ± SD.

(e) Effects of α-GalCer treatment of HFD-fed mice on metabolic parameters 10 days after treatment.

(f) Glucose tolerance test (GTT) was performed at 10 days after α-GalCer injection. Mice were administered 2g/kg glucose via i.p. injection after a 14 hr fast. Blood glucose was measured at 0, 15, 30, 60, and 120 after glucose injection. Data are mean ± SEM from n = 8–9 mice per group.

(g) HOMA-IR was assessed at 10 days after α-GalCer injection based on the fasting blood glucose and fasting insulin concentration using the equation, HOMA-IR= (glucose in mmol/L x insulin In mIU/mL)/22.5. Data are mean ± SEM from n = 8–9 mice per group.

(h) Adoptive transfer of GalCer-activated eWAT iNKT cells from HFD mice. On day 3 after α-GalCer treatment, iNKT cells were sort purified from eWAT SVF (~90% purity) of donor HFD mice and transferred by i.p. injection into recipient HFD mice (HFD+iNKT), alongside untreated HFD Ctrl or α-GalCer-treated HFD mice (HFD+GC). On day 4 post-transfer or post α-GalCer, eWAT SVF was isolated for $C_{12}FDG$ SA-βgal assay.

(i) Representative histograms of $C_{12}FDG$ fluorescence and gating for HFD Ctrl, HFD+iNKT and HFD+GC mice.

(j) Quantification of the percent of $C_{12}FDG^{Hi}$ subpopulation from the CD45$^-$ CD31$^-$ subset for each group of mice. Data are mean ± SD from n = 2 experiments.

*p < 0.05, **p < 0.005, ***p< 0.0005, one-way ANOVA.
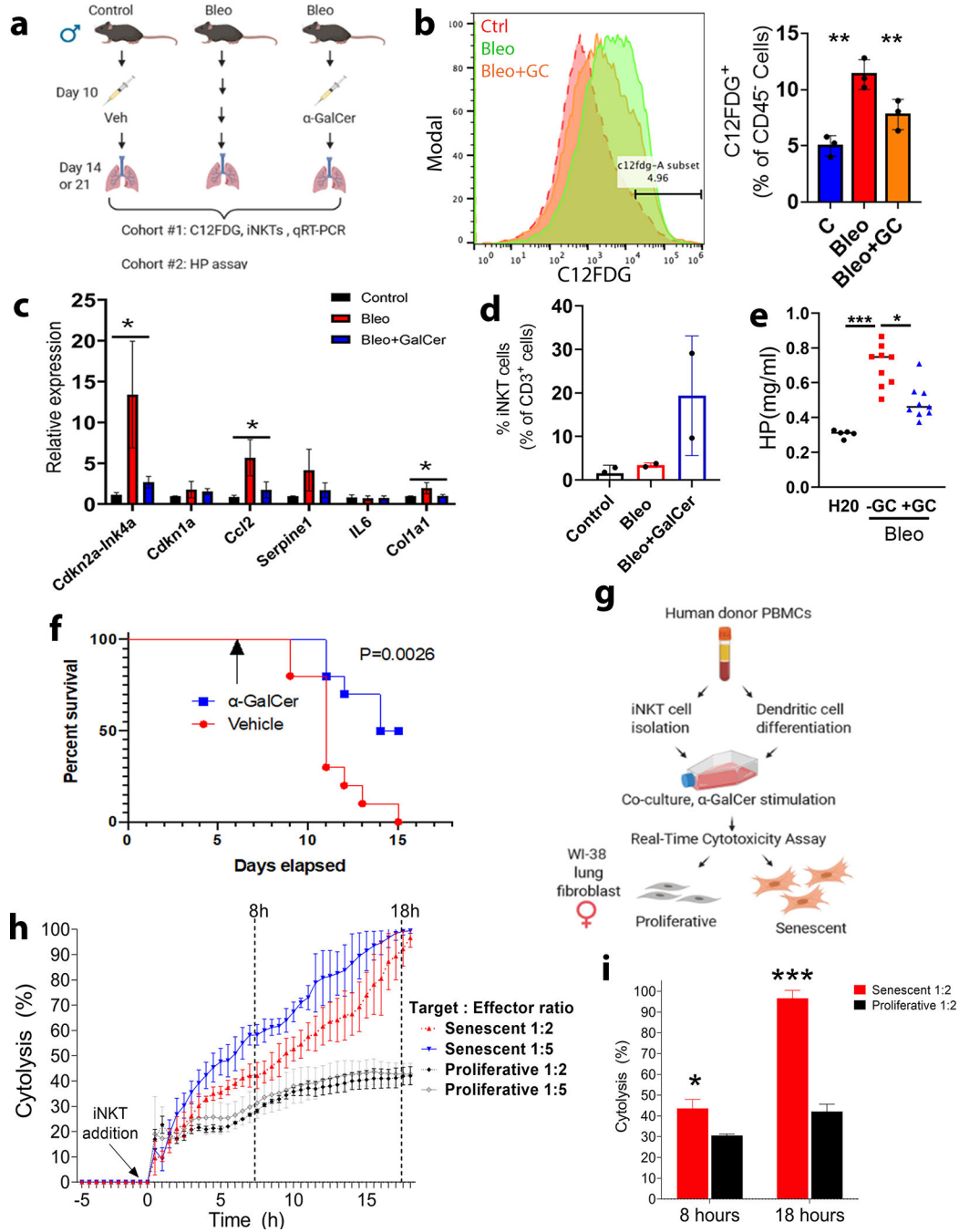
Figure 4. Activation of iNKT cells preferentially eliminates senescent cells in a murine lung injury model and in vitro using human cells

(a) Bleomycin was used to induce lung injury and a separate group of mice remained uninjured as controls. On day 10 post-injury α-GalCer was administered, or mice remained untreated, and control mice were administered vehicle. In cohort #1, day 14 post-injury mice lungs were harvested for analysis of senescent cells by $C_{12}FDG$ assay and qRT-PCR and enumeration of iNKTs. In cohort #2, mice were used for analysis of fibrosis on day 21.

(b) Representative histogram of C_{12}FDG fluorescence and quantifications of mean±SD from n = 3 mice per group in CD45$^-$ lung parenchymal cells.

(c) qRT-PCR of senescence and SASP in CD45-depleted lung cells, showing mean ± SD of n = 3 mice per group, *p < 0.05, one-way ANOVA.

(d) Percentages of iNKT cells as a proportion of T cells from the same mice as (b), mean ± SD of n = 2 mice per group.

(e) Quantification of fibrosis by hydroxyproline (HP) concentrations in Control (n = 5), Bleo (n = 10), and Bleo+GC (n = 10) mice per group, error bars are SD. ***p < 0.0005, *p < 0.05, one-way ANOVA Krusak-Wallis test.

(f) Kaplan Meier survival curve for mice injured with intratracheal bleomycin (4 U/kg) and injected with α-GalCer or vehicle at day 5 (arrow). N=10 mice per group. Significance calculated by Log-rank (Mantel-Cox) test.

(g) In vitro co-culture assay to monitor cytotoxicity using human iNKT cells isolated from donor PBMCs and WI-38 primary human lung fibroblasts. Dendritic cells differentiated from donor PBMCs were loaded with α-GalCer, while iNKTs were isolated from the PBMCs. WI-38 female lung fibroblasts were induced to senescence with etoposide or remained proliferative as a control. WI-38 cells were incubated with varying ratios of purified human iNKT cells. Changes in impedance were monitored with the XCelligence assay system and software was used to calculate percent cytolysis.

(h) Time course of XCelligence assay showing mean percent of cytolysis over 18 hours of the assay for the indicated samples. Each time-point measurement was from n = 3 biological replicates for each sample.

(i) Mean percent cytolysis at 8 h and 18 h for indicated 1:2 target-effector ratios (n = 3 biological replicates each), error bars are SD. *p < 0.05, ***p < 0.0005 one-way ANOVA.

KEY RESOURCES TABLE

REAGENT or RESOURCE	SOURCE	IDENTIFIER
Antibodies		
CD45 nanobeads	BioLegend	480028
Anti-mouse Cd45 APC (Clone 30F-11)	BioLegend	103112
Purified anti-mouse CD16/32 (2.4G2) antibody	UCSF antibody core	AM004-PURE
Anti-mouse Cd31-PECy7 (Clone 390)	BioLegend	102418
Cd1d-PE (Clone 1B1)	BioLegend	123509
Anti mouse Cd3-apc (clone 17A2)	BioLegend	100236
CD1D-PE Unloaded	NIH-Tetramer core	CD1D-PE Unloaded
TCR vα24 PE antibody	Beckman Coulter	IM2283
TCR vβ11 FITC antibody	Beckman Coulter	IM1586
Anti-iNKT Beads	Miltenyi Biotec, Inc.	130-094-842
CD1D-PE loaded PBS 57 (α-Galcer-analogue)	NIH-Tetramer core	mouse CD1d PBS-57
Bcl-xL (54H6) Rabbit mAb	Cell signaling	2764T
Anti-mouse IgG, HRP-linked Antibody #7076	Cell signaling	7076S
β-Tubulin	Millipore	MAB5564SP
Biological Samples		
eWAT of 22 weeks old c57bl/6 and C57BL/6 DIO male mice	This Paper	See Experimental Models: Organisms/Strains Section
Lungs from 10 weeks old c57bl/6 male mice	This Paper	See Experimental Models: Organisms/Strains Section
Primary cells from eWAT of 12 OR 22 weeks old c57bl/6 and C57BL/6 DIO male mice	This Paper	See Experimental Models: Organisms/Strains Section
Chemicals, Peptides, and Recombinant Proteins		
Bleomycin	Meitheal Pharmaceuticals Inc	NDC:71288-106-10
α-Galactosylceramide	HelloBio	HB3751
7-AAD	Cayman Chemical	400201
DAPI	Thermo	62248
C12-FDG	Makergene	M2888
ABT-737	adooq	A10255
IL2	Biolegend	589108
GM-CSF	Biolegend	572903
IL-4	Biolegend	574004
non-essential amino acid solution	Caisson Labs	NAL03-100ML
RPMI-1640	Corning®	10-040-CV
sodium pyruvate	Caisson Labs	PYL01-100ML
L-Glutamine	Corning®	25-005-CI
Mitomycin C	MedChem Express	HY-13316
Etoposide	Sigma	E1383
Fibronectin	abm	TM059

REAGENT or RESOURCE	SOURCE	IDENTIFIER
EMEM	VWR	76000-922
DNase	Roche	10104159001
Dispase	Thermo Fisher	17105041
Collagenase D	Roche	11088882001
BSA	Fisher	BP1600-100
FBS	Gemini	100-106
dPBS	Gibco	14190-144
ACK Lysis Buffer	Gibco	A10492-01
DMEM F/12	Gibco	11320082
RPMI 1640	Fisher/Life Tech	11875-093
Anti-Anti	Fisher Scientific	15-240-096
HEPES	Thermo	15630080
Penstrep	Life Technologies	15140122
DMEM	Gibco	11965118
Trizol	zymoresearch	R2050-1-200
Mojo Sort Buffer	Biollegend	480017
Tween 20	Fisher	142100
DMSO	Sigma	D2438
Glucose	Sigma	G5767
Chloramine T hydrate	Sigma	85739-100G
Isopropanol	Fisher scientific	A416-500
Trichloro acetic acid	Sigma	T6399-100G
Ehrlich's solution	Sigma	03891-250ML
Hydroxyproline standards	Sigma	H5534-10MG
HCl	Fisher scientific	144-500ml
Sodium acetate	Sigma	241245-500G
Cell Staining Buffer	BioLegend	420201
Humulin R Insulin	Eli Lilly	1325240
Critical Commercial Assays		
Senescence β-Galactosidase Staining Kit	Cell Signaling Technology	9860
RNA- Microprep Kit	Zymoresearch	R2062
qScript cDNA synthesis Kit	Quantabio	95048-100
FreeStyle Lite Glucose test strips	Abbott	LITE200
Septamate ᵗᵐ PBMC isolation system	STEMCELL Technologies	85460
Easysep Human Cd14 positive selection Kit	STEMCELL Technologies	17858
Power-Up SYBR	Fischer Scientific	A25743
E-Plate 96 PET	Agilent	300600900
Ultra Sensitive Mouse Insulin ELISA Kit	Crystal Chem	90080
Thermo Scientific™ Pierce™ ECL Western Blotting Substrate (ECL)	Fisher Scientific	PI32209

REAGENT or RESOURCE	SOURCE	IDENTIFIER
Deposited Data		
This study did not generate/analyze any datasets/code		
Experimental Models: Cell Lines		
WI-38 (ATCC® CCL-75™)	ATCC	ATCC® CCL-75™
Experimental Models: Organisms/Strains		
C57BL/6J	The Jackson Laboratory	000664
C57BL/6J DIO	The Jackson Laboratory	380050
B6(Cg)-Traj18tm1.1kro/J	The Jackson Laboratory	030522
Oligonucleotides		
Mouse Cdkn2a-Ink4a/P16 Forward	This Paper	GAACTCTTTCGGTCGTACCC
Mouse Cdkn2a-Ink4a/P16 Reverse	This Paper	AGTTCGAATCTGCACCGTAGT
Mouse Cdkn2d-Ink4d / P19/Cdkn2a-Arf Forward	This Paper	GCCGCACCGGAATCCT
Mouse Cdkn2d-Ink4d / P19/Cdkn2a-Arf Reverse	This Paper	TTGAGCAGAAGAGCTGCTACGT
Mouse Cdkn2b/P15 Forward	This Paper	AGATCCCAACGCCCTGAAC
Mouse Cdkn2b/P15 Reverse	This Paper	CCCATCATCATGACCTGGATT
Mouse Cdkn1a/P21 Forward	This Paper	GAACATCTCAGGGCCGAAAA
Mouse Cdkn1a/P21 Reverse	This Paper	TGCGCTTGGAGTGATAGAAATC
Mouse IL6 Forward	This Paper	ACCACGGCCTTCCCTACTTC
Mouse IL6 Reverse	This Paper	TTGGGAGTGGTATCCTCTGTGA
Mouse IL1β Forward	This Paper	CACAGCACATCAACAAG
Mouse IL1β Reverse	This Paper	GTGCTCTAGTCCTCATCCTG
Mouse IL1α Forward	This Paper	AAGAGACCATCCAACCCAGATC
Mouse IL1α Reverse	This Paper	CCTGACGAGCTTCATGAGTTTG
Mouse Cxcl10 Forward	This Paper	TCATCCTGCTGGGTCTGAGT
Mouse Cxcl10 Reverse	This Paper	GGACCGTCCTTGCGAGAG
Mouse Ccl2 Forward	This Paper	GTCTGTGCTGACCCCAAGAAG
Mouse Ccl2 Reverse	This Paper	TGGTTCCGATCCAGGTTTTTA
Mouse Serpine1 Forward	This Paper	GGACACCCTCAGCATGTTCA
Mouse Serpine1 Reverse	This Paper	CGGAGAGGTGCACATCTTTCT
Mouse Ppia Forward	This Paper	GTCTCCTTCGAGCTGTTTGC
Mouse Ppia Reverse	This Paper	AGCCAAATCCTTTCTCTCCA
Mouse Col1a1 Forward	This Paper	GACGCATGCCCAAGAAGACA
Mouse Col1a1 Reverse	This Paper	CTCGGGTTTCCACGTCTCAC
Mouse Hprt Forward	This Paper	CTGGTGAAAAGGACCTCTCG
Mouse Hprt Reverse	This Paper	TGAAGTACTCATTATCAAGGGCA
Software and Algorithms		
GraphPad Prism	GraphPad Software, Inc.	Version 6
Flowjo	Flowjo.com	Version 8
RTCA Software Pro	Agilent	

REAGENT or RESOURCE	SOURCE	IDENTIFIER
Other		
High Fat Diet	Research Diet Inc.	D12492